Click here to view PowerPoint presentation; Press Esc to exit

Bistatic STAP for Space-Based GMTI Radar

Braham Himed
AFRL/SNRT
26 Electronic Parkway
Rome, NY 13441 USA

Braham.Himed@rl.af.mil

Douglas A. Page
BAE Systems FRL/SNRT
26 Electronic Parkway
Rome, NY 13441 USA

Douglas.Page@baesystems.com

ABSTRACT

In this paper, we describe application of bistatic space-based radar (SBR) system for performing ground moving target indication (GMTI) surveillance. We consider a candidate system employing a space-based transmit platform at medium earth orbit (MEO) and an airborne receive platform. To separate slowly moving targets from the ground clutter, we employ specialized space-time adaptive processing (STAP). Our algorithm compensates for range dependence of clutter statistics using a combination of knowledge-aided (KA) processing and an expectation-maximization (EM) algorithm for estimating covariance matrices in non-stationary interference. Using simulated data for an 88.1° bistatic angle scenario with significant terrain variations and line of sight blockage present, we calculate the STAP signal-to-interference plus noise ratio (SINR) loss as a function of ground target azimuth and Doppler. Performance of our STAP algorithm is compared to that of ideal processing, standard STAP processing and Higher Order Doppler Warping (HODW). Our algorithm is seen to provide significantly better GMTI detection than both standard STAP and HODW.

1.0 INTRODUCTION

As described in Refs. [1-4], a bistatic space-based radar (SBR) system is a promising concept for affordable wide-area ground moving target indication (GMTI) surveillance. Using a transmit platform at medium earth orbit (MEO) allows coverage of the entire earth with only a small number of satellites [3]. A bistatic system allows the range to the receiver to be much smaller than the range from the transmitter, thus reducing the transmit power and antenna size required to detect ground targets.

To separate slowly moving targets from background interference, space-time adaptive processing (STAP) is often used in monostatic airborne GMTI radar systems. Performing STAP in bistatic SBR systems is challenging due to the clutter properties in such systems. The large satellite velocity of a space-based transmit platform produces a wide spread in clutter Doppler frequency, producing endo-clutter conditions over a wide range of target velocities. As was described in [4, 5], in a bistatic radar system, the clutter possesses

Himed, B.; Page, D.A. (2006) Bistatic STAP for Space-Based GMTI Radar. In *Bistatic-Multistatic Radar and Sonar Systems* (pp. 27-1 – 27-12). Meeting Proceedings RTO-MP-SET-095, Paper 27. Neuilly-sur-Seine, France: RTO. Available from: http://www.rto.nato.int/abstracts.asp.

significant angle-Doppler range dispersion. This produces inherent range dependence to the clutter covariance matrix, making estimation of the clutter statistics more difficult. In a bistatic system, the clutter ridge is also non-linear, thus increasing the rank of the covariance matrix relative to a monostatic radar system. The effects of bistatic geometry have been found to cause significant STAP degradation in bistatic airborne radar systems [4-6].

In real GMTI scenarios, there is also range-dependence of the clutter reflectivity due to the non-homogeneous nature of the terrain. Additionally, terrain height variations affect the angle-Doppler clutter characteristics, further increasing the range dependence of the clutter covariance matrix. Moreover, there may be several sources of interference, such as ground clutter from multiple range ambiguities and volumetric clutter such as from rain storms. In a bistatic system, each of these interference sources can have different range dependencies of the angle-Doppler curves; further challenging techniques that mitigate clutter non-stationarity.

Specialized techniques have already been developed for producing improved covariance estimates in airborne bistatic geometries. These include higher order Doppler warping (HODW) [7], derivative based updating (DBU) [8], and angle-Doppler compensation (ADC) [4]. HODW applies a range-dependent Doppler shift in order to compensate for clutter non-stationarity. DBU relies on a Taylor series expansion of the STAP weight vector as a function of range. The ADC technique [4] improves on HODW by incorporating both a temporal and a spatial shift into the range-dependent transformations.

In order to address the unique challenges presented by bistatic SBR GMTI systems, we apply an algorithm that incorporates knowledge of the bistatic geometry and terrain conditions into a set of range-dependent model covariance matrices. These covariance matrices feed a modified form of an expectation-maximization (EM) algorithm for covariance estimation in non-stationary interference. The approach, which will be referred to as knowledge-aided (KA) EM processing, can compensate for non-stationarity of both the clutter reflectivity and angle-Doppler characteristics. Moreover, since the approach employs an additive interference model, it can be used to simultaneously compensate for different range dependencies of multiple interference sources.

2.0 BISTATIC SBR SYSTEM AND SCENARIO DESCRIPTION

Table 1 lists the bistatic SBR system parameters assumed. The system parameters reflect a design meeting the requirements outlined in Ref. [3] for a SBR system performing wide area surveillance of ground targets. In [2, 9], the design of a bistatic SBR system employing a space-based transmitter and airborne receiver for GMTI surveillance was considered. The radar system parameters shown in Table 1 reflect a modification of the design presented in [9], corresponding to a medium earth orbit (MEO) rather than a low earth orbit (LEO) transmit platform.

In order to mitigate the effects of earth rotation and frequency dispersion over the 18 MHz bandwidth, time delay steering (TDS) [10] is employed on a pulse by pulse basis in each of the 36 antenna subarrays. The TDS reference location was assumed to be the same as the center of the antenna footprint on the ground. The STAP degrees of freedom (DOF) for the GMTI system were selected using PRI-staggered post-Doppler processing with 3 temporal DOFs. We have found this algorithm to provide effective STAP performance with a minimum number of degrees of freedom. The latter is especially important in bistatic systems, as the size of the range training window required for good covariance estimation is proportional to the number of adaptive degrees of freedom. In bistatic systems, the size of the training window, and hence the number of adaptive DOFs, should be kept small to reduce covariance estimation errors due to inherent range variation of the

angle-Doppler clutter characteristics.

Table 1 Assumed Bistatic SBR System and Scenario Parameters

Coverage rate	250 km by 250 km every 10 sec for a 10 m^2 target RCS (independent of aspect)
Transmitter altitude	10,000 km (MEO)
Radar frequency	C-band
Transmit antenna size	50 m by 20 m
Average power	3 kW
CPI	45 ms
PRF	1 kHz
Receive altitude	20 km
Receive platform speed	200 m/s
Receive antenna size	2 m by 0.5 m
Antenna configuration	36 vertical subarrays
STAP configuration	Post-Doppler PRI-staggered processing (3 staggers)

In this paper, we consider a bistatic geometry in which the bistatic angle (defined as the angle between the line of sight from the center of the transmit beam to the transmitter and the line of sight to the receiver) is 88.1°. Table 2 summarizes the parameters for the simulated scenario. Note that the 4.8° receive grazing angle corresponds to approximately a 200 km range from the receiver to the target position.

Table 2 Simulated bistatic scenario parameters

Look direction of transmitter (at TDS reference location)	West
Grazing angle to transmitter (at TDS reference location)	23°
Heading of transmit ground track	South
Look direction of receiver (at TDS reference location)	North
Grazing angle to receiver (at TDS reference location)	4.8°
Heading of receive ground track	West

In order to simulate the effects of bistatic SBR clutter, ground scatterer locations within each bistatic range-gate were determined. Each range-gate corresponds to a constant time of arrival surface, which is an ellipsoid with foci at the transmit and receive locations. The intersection of the range ellipsoids with the earth's surface defines the locations of ground clutter scatterers in each range-gate. We also simulated the effects of terrain

height variations using level 1 digital terrain elevation data (DTED).

For the simulated scenario, 3 range ambiguities of ground clutter returns are present. Figure 1 shows the visible portions of the range ambiguities in the target range-gate on a latitude-longitude display. The receive platform location and transmit antenna footprint are also shown. Note that the higher range ambiguities are well outside the antenna footprint, which results in attenuated returns from the ambiguities.

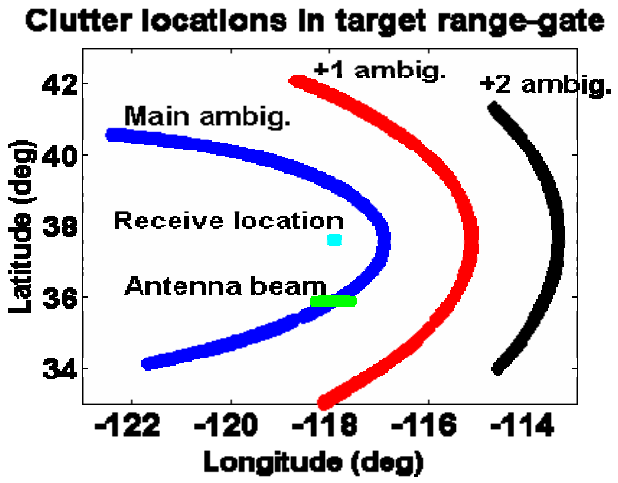

Figure 1 Visible portions of the 3 simulated range ambiguities, receive platform location, and antenna footprint

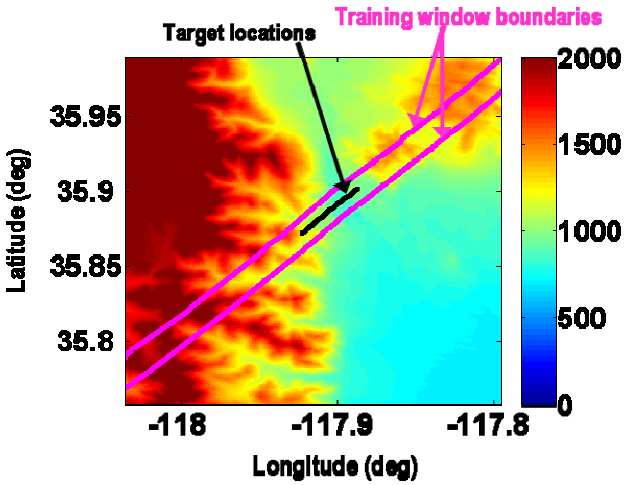

Figure 2 Terrain height map (meters) on expanded scale showing simulated target locations and boundaries of STAP training window

Figure 2 shows the terrain height profile and assumed target locations on an expanded scale within the antenna footprint in the main ambiguity. The target locations span approximately 1° in azimuth with respect to the receive platform. The boundaries of the STAP training window, which spanned 145 bistatic range-gates, are also shown in Figure 2.

The upper portion of figure 3 shows the angle-Doppler contours of the visible clutter in each range ambiguity in the target range-gate. Note the significant dispersion across the range ambiguities produced by the bistatic geometry (in a monostatic radar with no crab angle, the angle-Doppler contour is a straight line). The lower portion of Figure 3 shows the contours in the main range ambiguity for 3 range-gates on an expanded scale near the origin (which is the target location). The location of the peak of the clutter spectrum, or clutter spectral center [4], is also shown for each range-gate.

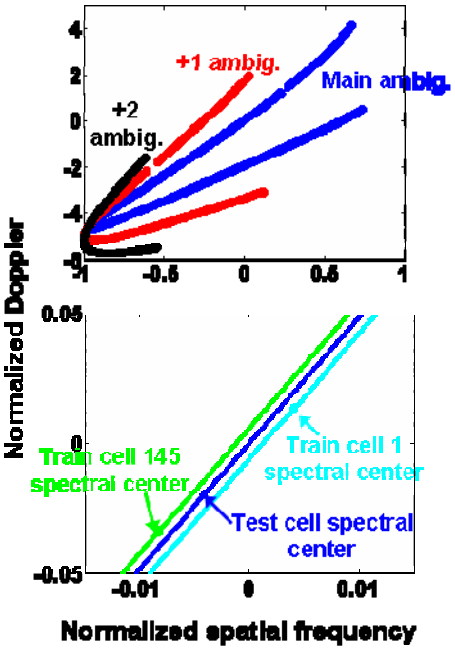

Figure 3 Doppler-angle contours of the 3 simulated range ambiguities (top plot). The lower plot shows an expanded portion of 3 range-gates in the main range ambiguity. The locations of the clutter spectral centers are also shown on the lower plot.

Even though the dispersion of the angle-Doppler contours and clutter spectral centers across the training window appears to be small, it is enough to cause significant degradation in standard sample matrix inversion (SMI) STAP. The latter forms a covariance matrix estimate by averaging over the range training window. The fact that the clutter contours and spectral centers are varying with range produces significant error in the standard SMI covariance estimate. This in turn, causes broadening of the nulls in the STAP filter response and degraded signal to interference plus noise ratio (SINR) loss on slowly moving targets. Note that the spectral centers in Figure 3 are not uniformly spaced across the training window. This is due to the combined effects of the bistatic geometry and the terrain.

Complex radar returns from the clutter scatterers in each bistatic range-gate were simulated and used to evaluate the performance of different STAP techniques. The return amplitudes of the scatterers were calculated using the bistatic radar range equation. To determine the bistatic scattering coefficient, the monostatic-bistatic equivalence theorem was employed with a -10dB constant-gamma model.

Figure 4 shows the calculated SINR loss as a function of target velocity (along North) and target azimuth offset (relative to the center of the target azimuth interval) for a matched filter; i.e. using the ideal covariance matrix to compute the STAP weight vector. Note that there is some shadowing, or line of sight blockage, at certain azimuth angles. The clutter null, centered on zero velocity, appears to be approximately independent of azimuth for ideal STAP processing (apart from target shadowing effects).

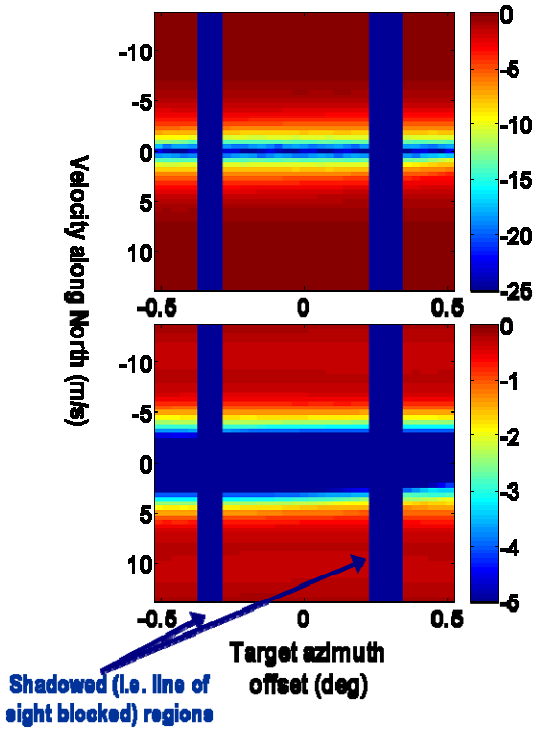

Figure 4 Simulated SINR loss as a function of target velocity and target azimuth offset for ideal processing using the known covariance over 25 dB (top) and 5 dB loss intervals

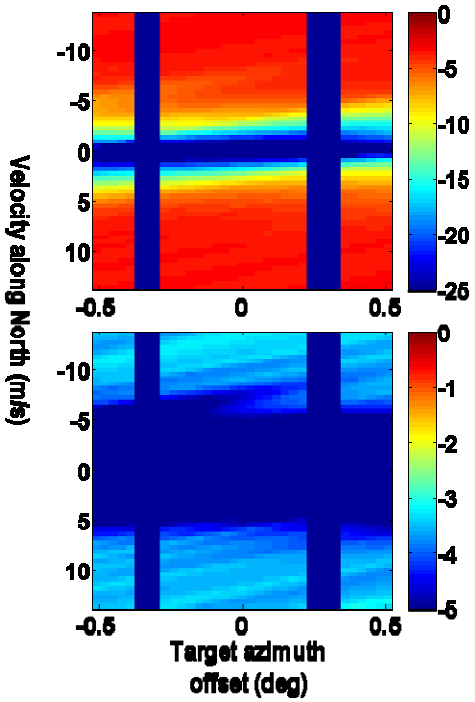

Figure 5 Simulated SINR loss as a function of target velocity and target azimuth offset for standard STAP over 25 dB (top) and 5 dB (bottom) loss intervals

Figure 5 shows the corresponding result for standard SMI STAP. Note the significant broadening of the SINR loss null around zero velocity compared to ideal processing. Additionally, there is noticeable variation of the clutter null boundaries with target azimuth offset.

We define the minimum detectable velocity (MDV) for target motion in a given direction as the velocity producing a -5dB SINR loss threshold. The latter corresponds to a 16dB SINR for a $10m^2$ target. Figure 6 shows the MDV for target motion along North (positive velocity) and South (negative velocity) as a function of target azimuth offset, for both ideal processing and standard SMI STAP. Standard SMI STAP is observed to produce an MDV that is highly degraded over ideal STAP, by more than a factor of 2 at some azimuth angles. In terms of GMTI tracking performance, such degradation could translate into increased number of track dropouts, reduced time in track, increased misassociations due to degraded target parameter estimates, and an increased number of false tracks if the detection threshold were lowered to maintain tracks on slowly moving targets.

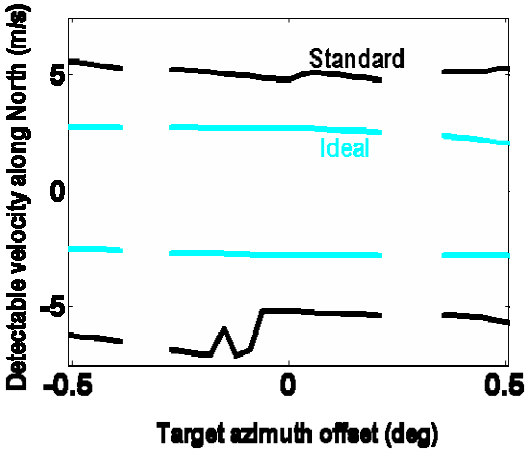

Figure 6 MDV for target motion along North (positive velocity) and South (negative velocity) as a function of target azimuth offset for ideal STAP (cyan, middle curves) and standard SMI STAP (black, top and bottom curves)

3.0 KNOWLEDGE-AIDED EM STAP PROCESSING

A block diagram of our KA-EM STAP approach is shown in Figure 7.

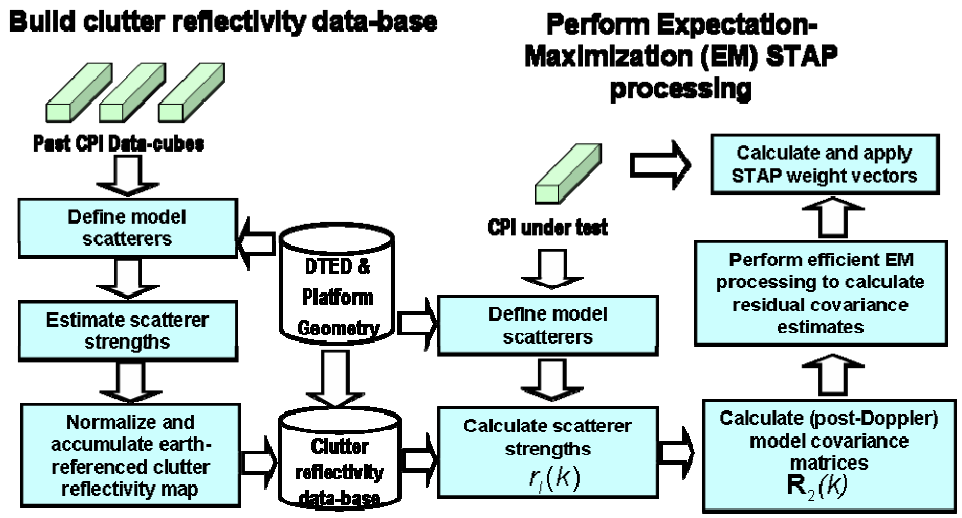

Figure 7 Block diagram of KA-EM STAP processing

The left side of the diagram shows how we estimate the spatial variation of clutter reflectivity. As the surveillance region is revisited periodically, multiple coherent processing intervals (CPIs) are used to build a data base containing knowledge of the spatial variation of clutter reflectivity. The algorithm described in Ref. [11] was modified to produce improved accuracy in bistatic SBR systems. In each range-gate *k* of each of the CPI data-cubes, a set of model point scatterers spanning a specified Doppler extent is defined. The locations of these scatterers on the ground are then determined. The scattering strengths of the model scatterers are

estimated from the data using a single-stage EM procedure [12]. Normalized scatterer reflectivity is then computed, which takes out the effects of antenna gain and cell area (both of which change from CPI to CPI). Once the scatterer reflectivities are determined, an earth-referenced clutter reflectivity map is formed representing average reflectivity as a function of latitude and longitude.

The right hand side of the block diagram shown in Figure 7 describes the EM processing that is performed on the CPI under test. The EM approach [13] to covariance estimation in non-stationary interference models the space-time data vector in each range-gate *k* as the sum of two terms:

$$\boldsymbol{x}(k) = \boldsymbol{x}_1(k) + \boldsymbol{x}_2(k), \tag{1}$$

with

$$\left\langle \boldsymbol{x}_1(k)\,\boldsymbol{x}_1^H(k) \right\rangle \equiv \boldsymbol{R}_1 \text{ and } \left\langle \boldsymbol{x}_2(k)\,\boldsymbol{x}_2^H(k) \right\rangle \equiv \boldsymbol{R}_2(k). \tag{2}$$

The stationary term is assumed to be a complex, zero mean circular Gaussian random variable, with a range independent covariance $\boldsymbol{R}_1$ that is to be estimated. An initial estimate of $\boldsymbol{R}_1$ is assumed to be available. The non-stationary term is also assumed to be a complex, zero mean circular Gaussian, but has a known covariance $\boldsymbol{R}_2(k)$ that varies with range. As shown in Figure 7, the reflectivity estimates determined from the multi-CPI clutter database described above are used to form the model covariance matrices $\boldsymbol{R}_2(k)$.

In the algorithm described in Ref. [14], an efficient EM procedure is defined to update the stationary covariance as follows:

$$\boldsymbol{R}_1^{(q+1)} = \boldsymbol{R}_1^{(q)} + \boldsymbol{v}^{(q)}\boldsymbol{v}^{(q)H}, \tag{3}$$

where *q* is the iteration index and $\boldsymbol{v}^{(q)}$ is a vector representing the updated knowledge of the stationary interference on the current iteration. As shown in Ref. [14] the vector $\boldsymbol{v}^{(q)}$ is proportional to an eigenvector of a certain matrix $\boldsymbol{M}$. This matrix depends on the measured data vectors $\boldsymbol{x}(k)$, the model covariance matrices $\boldsymbol{R}_2(k)$, and the stationary covariance estimate $\boldsymbol{R}_1^{(q)}$. The eigenvector having the largest eigenvalue is selected, and an equation determining the norm of the vector $\boldsymbol{v}^{(q)}$ is also given in Ref. [14].

Once the EM iterations have been completed, the STAP weight vector in the test cell k_0 is then computed using

$$\boldsymbol{w} = \left[\boldsymbol{R}_1^{(Q)} + \boldsymbol{R}_2(k_0) \right]^{-1} \boldsymbol{s}_t, \tag{4}$$

where *Q* is the last iteration index and $\boldsymbol{s}_t$ is the target steering vector. This weight vector is then used to perform adaptive filtering.

To apply this technique to the bistatic SBR problem, we compute non-stationary covariance matrices using

$$\boldsymbol{R}_2(k) = \sum_i r_i(k)\,\boldsymbol{s}_i(k)\boldsymbol{s}_i^H(k), \tag{5}$$

where i is an index labelling a set of point scatterers along the bistatic clutter ridge. Here, $r_i(k)$ is the estimated strength of model scatterer i using the earth-referenced clutter reflectivity map. To determine the post-Doppler space-time steering vectors $\mathbf{s}_i(k)$ of the scatterers, their spatial and temporal frequencies are computed using knowledge of the platform parameters and terrain elevation. Note that these frequencies are generally located on a non-linear angle-Doppler contour. This allows, for example, compensation for a range-dependent mismatch of both the slope and location of the angle-Doppler contours.

The KA-EM approach has the significant advantage of being able to simultaneously compensate for multiple interference sources, which may have different dependencies on bistatic range. For example, if range or Doppler ambiguities are expected to produce significant returns, model scatterers may be defined in these ambiguities in addition to the main ambiguity. This allows compensation for the different amounts of clutter range variation in each range and Doppler ambiguity producing significant returns.

4.0 PERFORMANCE COMPARISON

The KA-EM procedure described in the last section was applied to the simulated bistatic SBR scenario discussed in section 2. A total of 6 CPI datacubes were generated, corresponding to a 10 second revisit time per CPI. KA- EM processing was implemented using a clutter reflectivity map with 10m resolution, and the number of EM iterations employed was $Q = 6$.

Figures 8 and 9 show the SINR loss results for HODW and KA-EM algorithms respectively. While HODW is observed to produce an SINR loss characteristic that is improved over that of standard SMI STAP (Figure 5), KA-EM is observed to provide a significantly narrower clutter null than HODW. Figure 10 shows the MDV results for HODW and KA-EM compared to that of ideal and standard STAP processing. The KA-EM algorithm is seen to provide near-ideal performance over the entire range of target azimuth angles. The MDV of HODW is seen to be higher than that of KA-EM by 40-70% depending on target azimuth and direction of motion. Additionally, HODW is seen to produce an MDV that varies more with target azimuth than KA-EM. This is a sign that the clutter has not been completely nulled, and the residual clutter level varies depending upon the target location. This in turn is due to the assumption made by HODW that a simple Doppler shift (depending on range and Doppler filter) can compensate for clutter non-stationarity. The KA-EM does not make this assumption. By placing model scatterers along the nonlinear angle-Doppler contours in each range-gate, and providing adaptive estimates of their scattering strengths, the KA-EM algorithm is able to optimally mitigate range dependence of the clutter characteristics due to the bistatic geometry and terrain height variations.

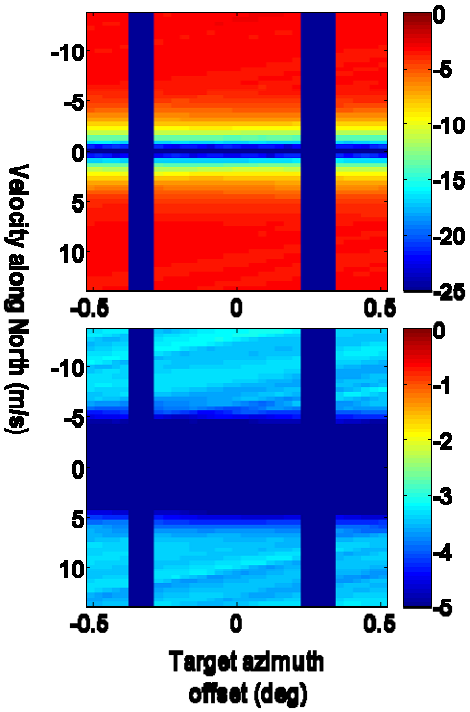

Figure 8 Simulated SINR loss as a function of target velocity and target azimuth offset for HODW over 25 dB (top) and 5 dB (bottom) loss intervals

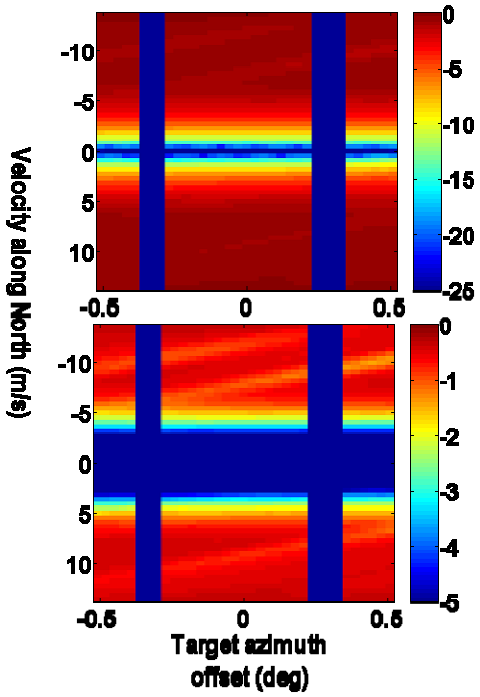

Figure 9 Simulated SINR loss as a function of target Doppler offset and target azimuth offset for KA-EM processing over 25 dB (top) and 5 dB (bottom) loss intervals

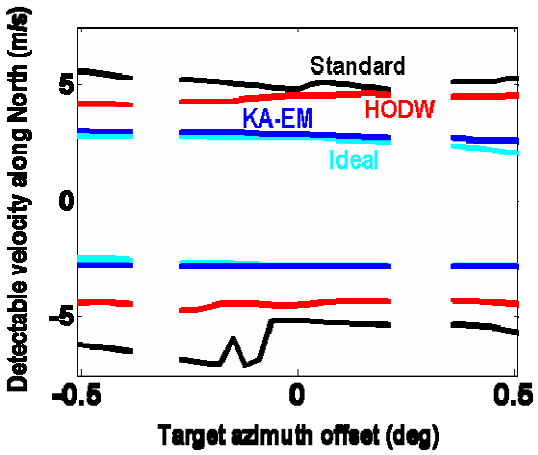

Figure 10 MDV as a function of target azimuth offset of ideal STAP (middle, cyan curves), standard STAP (top and bottom, black curves), HODW (second from top and second from bottom, red curves), and KA-EM STAP (blue curves)

5.0 REFERENCES

[1] Guttrich, G.L., Sievers, W.E., and Tomljanovich, N.M., "Wide Area Surveillance Concepts Based on Geosynchronous Illumination and Bistatic Unmanned Airborne Vehicles or Satellite Reception", *Proc. 1997 IEEE National Radar Conf*erence, pp. 126-131.

[2] Hartnett, M.P., and Davis, M.E., "Bistatic Surveillance Concept of Operations", *Proc. 2001 IEEE National Radar Conference*, pp. 75-80.

[3] Davis, M.E., "Space-Based Radar Core Technology Challenges for Affordability", Proc. *2001 Core Technologies for Space Systems Conference*, Colorado Springs, Colorado, Nov. 28-30, 2001.

[4] Himed, B., Zhang, Y., and Hajjari, A., "STAP with Angle-Doppler Compensation for Bistatic Airborne Radars", *Proc. 2002 IEEE National Radar Conference*, pp. 311-317.

[5] Himed, B., Michels, J.H., Zhang, Y., "Bistatic STAP Performance Analysis in Radar Applications", *Proc. 2001 IEEE National Radar Conference*, pp. 198-203.

[6] Melvin, W.L., Callahan, M.J., Wicks, M.C., "Bistatic STAP: Application to Airborne Radar", *Proc. 2002 IEEE National Radar Conference*, pp. 1-7.

[7] Pearson, F., and Borsari, J., "Simulation and Analysis of Adaptive Interference Suppression for Bistatic Surveillance Radars", *Proc. 9th Annual Adaptive Sensor Array Processing Workshop*, 13-14 March 2001.

[8] Zatman, M., "Performance Analysis of the Derivative Based Updating Method", *Proc. 9th Annual Adaptive Sensor Array Processing Workshop*, 13-14 March 2001.

[9] Hartnett, M.P., and Davis, M.E., "Operations of an Airborne Bistatic Adjunct to Space Based Radar", *Proc. 2003 IEEE National Radar Conference*, pp. 133-138.

[10] Rabideau, D., and Kogon, S., "A Signal Processing Architecture for Space-Based GMTI Radar", *Proc. 1999 IEEE National Radar Conf*erence, 20-22 April 1999.

[11] Page, D.A., Scarborough, S., Owirka, G., and Crooks, S., "Improving Knowledge-Aided STAP Performance Using Past CPI Data", *Proc. 2004 IEEE National Radar Conference*, pp. 295-300.

[12] Page, D., Himed, B., Davis, M.E., "Higher Order Clutter Mitigation in Bistatic, Space-Based Radar Systems using a Knowledge-Aided STAP Approach", *Proc. 2006 IEEE National Radar Conference*, Verona, NY April 24-27, 2006, pp. 459-464

[13] Fuhrmann, D.R., "Covariance Estimation in Non-stationary Interference", *Proc. 1993 Asilomar Conf. on Signals, Systems, and Computers*, pp. 1172-1175.

[14] Page, D., Himed, B., Davis, M.E., "Improving STAP Performance in Bistatic Space-Based Radar Systems using an Efficient Expectation-Maximization Technique", *Proc. 2005 IEEE International Radar Conference*, Arlington, VA, May 9-12, 2005, pp. 109-114.